Available online at www.sciencedirect.com

ScienceDirect

Ceramics International 41 (2015) 14293–14298

CERAMICS INTERNATIONAL

www.elsevier.com/locate/ceramint

Hydrothermally assisted synthesis of $YMnO_3$

Z. Branković[a,b,*], G. Branković[a,b], M. Počuča-Nešić[a], Z. Marinković Stanojević[a], M. Žunić[a,b], D. Luković Golić[a], R. Tararam[b], M. Cilense[b], M.A. Zaghete[b], Z. Jagličić[c,d], M. Jagodič[c], J.A. Varela[b]

[a]*Institute for Multidisciplinary Research, University of Belgrade, Kneza Višeslava 1a, 1030 Belgrade, Serbia*
[b]*Instituto de Química, Universidade Estadual Paulista-UNESP, R. Prof. Francisco Degni, n. 55, 14800-900 Araraquara, SP, Brazil*
[c]*Institute of Mathematics, Physics and Mechanics, Jadranska 19, 1000 Ljubljana, Slovenia*
[d]*Faculty of Civil and Geodetic Engineering, University of Ljubljana, Jamova 2, 1000 Ljubljana, Slovenia*

Received 27 May 2015; received in revised form 8 July 2015; accepted 10 July 2015
Available online 17 July 2015

Abstract

In this work single phase hexagonal $YMnO_3$ powders were prepared starting from $Y(CH_3COO)_3 \cdot xH_2O$, $Mn(CH_3COO)_2 \cdot 4H_2O$, $KMnO_4$ and KOH using methods of conventional (280 °C for 6 h) or microwave assisted hydrothermal synthesis (200 °C for 2 h) followed by calcination at 1200 °C for 2 h. According to FESEM analysis the calcined powders consisted of submicronic $YMnO_3$ particles, which were uniform in shape and size. Ceramic samples were obtained by sintering the as-synthesized powders at 1400 °C for 2 h. XRD analysis confirmed the presence of the single phase hexagonal $YMnO_3$. SEM analysis showed a dense and homogeneous microstructure with typical inter- and intra-grain cracks. Magnetic measurements indicated ferrimagnetic properties that were explained by non-stoichiometry of the obtained compound and an excess of manganese that was confirmed by ICP analysis.

Keywords: Yttrium manganite; Hydrothermal synthesis; Phase evolution; Magnetic measurements

1. Introduction

The main characteristics of the magnetoelectric materials are that they display simultaneously ferroelectric and ferromagnetic polarizations in the same phase. This coupling between ferroelectric and magnetic domains opens possibilities for many new applications [1,2]. Although complex perovskites can exhibit many interesting properties, such as magnetism, ferroelectricity or colossal magnetoresistance, there are only few perovskites which are multiferroics [3]. Manganites, such as $BiMnO_3$ or $REMnO_3$ (RE=rare earth), have been recognized as an important class of the multiferroic materials.

$YMnO_3$ and the rare earth (RE) manganites, (RE=Ho, Er, Tm, Yb, and Lu) can crystallize in either orthorombic or hexagonal perovskite type crystal structure depending on ionic radius size of RE. Stability of the orthorhombic structure (space group *Pnma*) decreases and the hexagonal structure of these manganites (space group $P6_3cm$) becomes more probable when RE is changing from Ho to Lu [3]. $YMnO_3$ can adopt both structures, but the orthorhombic phase can be obtained only by special synthesis methods, for example soft chemical method or mechanochemical synthesis [3–5]. The orthorhombic $YMnO_3$ exhibits an incommensurate antiferromagnetic transition at ~40 K (T_N – Néel temperature) and the ferroelectric transition at about 30 K [6,7]. The hexagonal $YMnO_3$ displays ferroelectric and antiferromagnetic properties with a strong coupling between them below 75 K [8].

It is well known that properties of materials can be significantly different in nanostructures and thin films in comparison with bulk or powders. There are several articles that report on the

*Corresponding author at: Institute for Multidisciplinary Research, University of Belgrade, Kneza Višeslava 1a, 11030 Belgrade, Serbia. Tel.: +381 11 2085043; fax: +381 11 2085038.
E-mail address: zorica.brankovic@imsi.bg.ac.rs (Z. Branković).

http://dx.doi.org/10.1016/j.ceramint.2015.07.060
0272-8842/

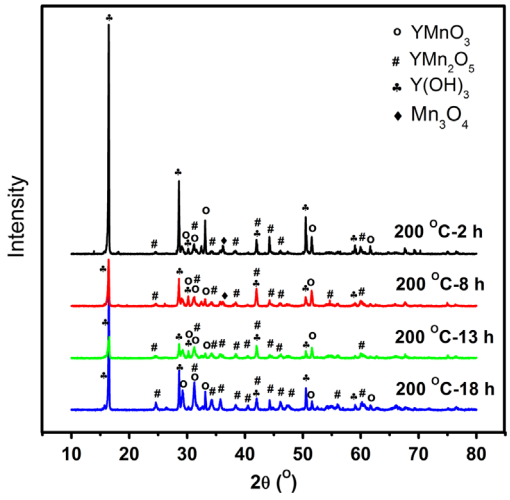

Fig. 1. XRD patterns of powders obtained by microwave-assisted hydrothermal synthesis for different reaction times.

size dependence of the microstructural, electric and magnetic properties of $YMnO_3$ [8–10]. In those investigations solid state synthesis and several chemical methods were used to obtain $YMnO_3$ samples with various grain sizes. The solid state synthesis of $YMnO_3$ requires very long procedure with repeated heating and grinding [9]. That is the reason why so many researchers have tried to find a simple and reproducible method for $YMnO_3$ synthesis, such as hydrothermal method [4,11]. It has many advantages like low reaction temperature and easy variation of synthesis conditions including temperature, pressure, pH, atmosphere etc. Nevertheless, there are only few articles about hydrothermal synthesis of $YMnO_3$, which are insufficient to judge the method efficiency [4,11,12].

The aim of this work was to investigate the phase evolution during hydrothermal synthesis of $YMnO_3$ and to propose optimal synthesis conditions for preparation of pure hexagonal $YMnO_3$ powders and ceramics.

2. Experimental

Precursor solution for the hydrothermal synthesis of $YMnO_3$ (YMO) was prepared starting from $Y(CH_3COO)_3 \cdot xH_2O$, Mn $(CH_3COO)_2 \cdot 4H_2O$, $KMnO_4$ and KOH, the method analogous to one proposed by Y. Wang and co-authors [12] for some other rare earth manganites and also by H.W. Zheng and co-authors [11] for $YMnO_3$. Starting yttrium and manganese compounds were dissolved in stoichiometric ratios in distilled water under magnetic stirring at room temperature and then KOH was added. Stoichiometric ratios were calculated based on chemical reaction that was expected to take place during the hydrothermal treatment [12]:

$$5Y(NO_3)_3 + KMnO_4 + 4MnCl_2 + 22KOH \rightarrow 5YMnO_3 + 15KNO_3 + 8KCl + 11H_2O \quad (1)$$

The hydrothermal synthesis was performed in two types of autoclaves: microwave assisted teflon-lined autoclave for temperatures up to 200 °C and stainless steel autoclave for higher temperatures from 230 to 280 °C. Duration of the hydrothermal treatment was also varied (2–48 h).

The obtained powders were calcined at different temperatures (900–1200 °C) to investigate the influence of temperature on phase composition and crystallinity. The powders were uniaxially pressed into pellets (6 mm diameter) at 687 MPa. Further, discs were sintered at 1400 °C for 2 h. Both the powders and the sintered samples were characterized by X-ray powder diffraction analysis (XRD, Rigaku DMax 2500 PC), field emission scanning electron microscopy (FESEM, Jeol JSM 6330 F), scanning electron microscopy (SEM, TESCAN Vega 3SB), density measurements, inductively coupled plasma analysis (ICP, Thermo Scientific iCAP 6500 Duo ICP) and magnetic measurements (magnetization vs. temperature and magnetic fields). The magnetic measurements of the $YMnO_3$ powder and sintered samples were carried out with a SQUID MPMS-XL-5 magnetometer from Quantum Design. The zero-field-cooled (ZFC) and field-cooled (FC) magnetization vs. temperature curves were studied in the temperature range 2–300 K in a magnetic field of 100 Oe, while isothermal magnetization measurements were recorded between −50 and 50 kOe at 5 K.

3. Results and discussion

The microwave-assisted hydrothermal synthesis at 200 °C was performed for different time periods, from 2 to 18 h. XRD patterns of the resulting powders showed that this temperature was insufficient for the preparation of pure $YMnO_3$ and also that prolongation of synthesis time did not result in phase pure $YMnO_3$ (Fig. 1). All synthesized samples contained the same phases: $Y(OH)_3$ (JCPDF 83–2042), Mn_3O_4 (JCPDF 75-1560), YMn_2O_5 (JCPDF 34-0667) and $YMnO_3$ (JCPDF 25-1079). Only the relative amounts of these phases were changed: prolongation of time resulted in higher amount of YMn_2O_5, but not in transformation of YMn_2O_5 to $YMnO_3$.

Zheng and co-workers [11] reported formation of pure $YMnO_3$ after hydrothermal treatment at 230 °C for 48 h. In our experiments, variation of synthesis temperature (230–280 °C) for different times (up to 48 h) did not yield pure $YMnO_3$ phase (Fig. 2), but mixture of $Y(OH)_3$, $YMnO_3$ and YMn_2O_5. Obviously, some parameters such as concentration, pH and filling capacity are very important and probably were very different in these two experiments. On the other hand, this is in accordance with the results published by Stampler and co-workers [4]. They found that YMn_2O_5 would be formed before $YMnO_3$ at temperatures lower than 300 °C and could be transformed to $YMnO_3$ phase during hydrothermal synthesis only at temperatures significantly higher than 300 °C. For example, they performed synthesis at 350 °C for 48 h.

SEM analysis of hydrothermally synthesized powders showed presence of several phases, and EDS analysis confirmed the presence of the same phases as identified by XRD (Fig. 3). Large rods, more than 10 μm in length were identified as $Y(OH)_3$, the dark gray phase consisted mainly of Mn_3O_4, while the nanosized columnar grains were identified as YMn_2O_5. Small quantity of $YMnO_3$ in these samples made

identification by EDS difficult, and it was hard to distinguish it from YMn_2O_5.

Apparently, the percentage of YMn_2O_5 increases with prolongation of time of hydrothermal treatment. SEM results of powders treated at 280 °C for 6 h showed the presence of particles differing in shape and size (Fig. 4a), but it could be seen that powder mainly consists of typical columnar grains of YMn_2O_5 (Fig. 4b).

Although our hydrothermal syntheses resulted in a mixture of phases, we found that after calcination at 1200 °C for 2 h the powders hydrothermally treated only for 2 h crystallized in a pure $YMnO_3$ hexagonal phase (Fig. 5). From the energy consumption point of view this is a more efficient method than the solid state synthesis that includes several steps of heating, grinding and reheating at temperatures higher than 1200 °C for few days in total, or hydrothermal synthesis for 48 h at 350 °C. Investigation of the influence of calcination conditions on phase composition showed that the temperatures lower than 1200 °C were insufficient for transformation to pure $YMnO_3$ (Fig. 5).

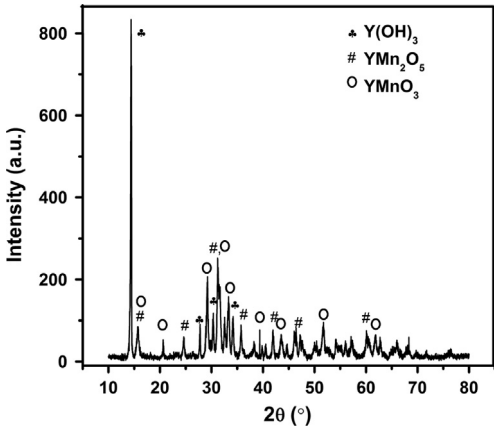

Fig. 2. XRD pattern of the powder synthesized at 280° for 48 h.

After calcination at 1200 °C for 2 h, only $YMnO_3$ particles were obtained (Fig. 6). Thus, joint effects of the hydrothermal treatment and calcination resulted in formation of the fine homogeneous powder consisting of small aggregates of several grains.

Alternatively, the powders hydrothermally treated at 200 °C and 280 °C were sintered at 1400 °C for 2 h without previous calcination, and the pure hexagonal $YMnO_3$ phase was also obtained (Fig. 7). The optimal sintering conditions were determined by dilatometric measurements which showed that an intensive shrinkage started at 1100 °C and continually proceeded up to 1400 °C. Evidently, any further increase in temperature of the hydrothermal treatment can not give any benefits in the synthesis of $YMnO_3$. Accordingly, the hydrothermal treatment at 200 °C and sintering at 1400 °C for 2 h without calcination step can be recommended as the optimal and most energy efficient method for preparation of $YMnO_3$ ceramics.

Relative densities of the samples sintered at 1400 °C for 2 h reached 95% of the theoretical density. A typical SEM micrograph of sintered YMO ceramics obtained by the hydrothermally assisted method was shown in Fig. 8 and

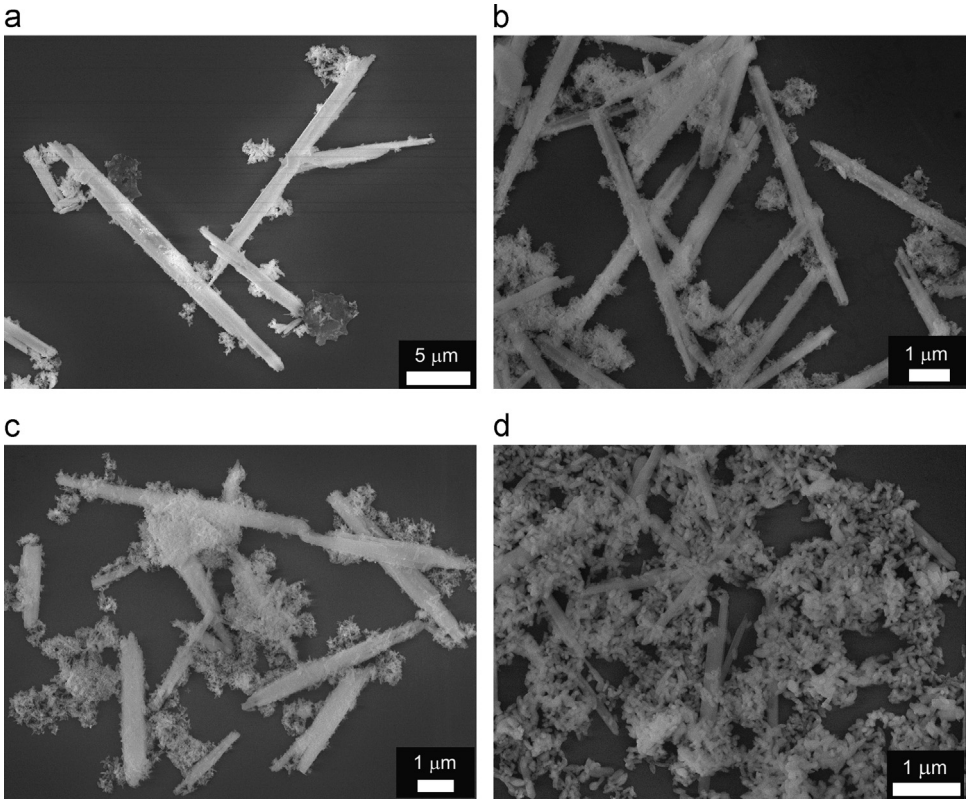

Fig. 3. SEM micrographs of the powders hydrothermally treated at 200 °C for: (**a**) 2 h, (**b**) 4 h, (**c**) 8 h and (**d**) 13 h.

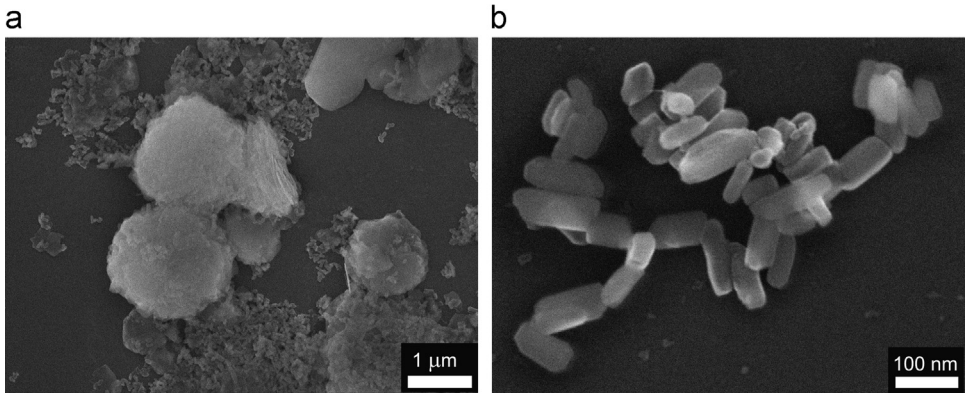

Fig. 4. (**a**) SEM micrograph of the hydrothermally synthesized powder – synthesis conditions: 280 °C for 6 h, and (**b**) high magnification micrograph of the same powder.

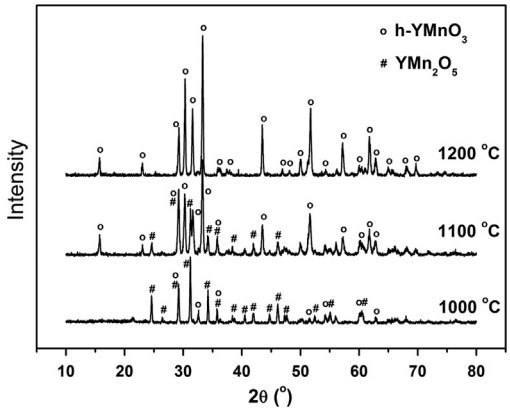

Fig. 5. XRD patterns of the powders hydrothermally treated at 200 °C for 2 h and calcined at 1000–1200 °C for 2 h.

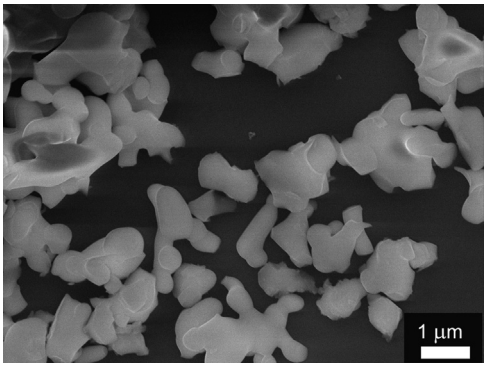

Fig. 6. SEM micrograph of the hydrothermally synthesized and calcined YMO powder.

confirmed that highly dense microstructure was obtained. Presence of both inter- and intra-granular cracks was also observed, as it has been already reported by other authors [13,14]. The sintering of YMO to obtain crack-free ceramics should be additionally investigated, and probably some alternative sintering methods should be considered as a possible solution of this common problem.

The results of magnetic measurements of the sintered YMO sample are given in Fig. 9. On account of being very sensitive these measurements can reveal the traces of some magnetic

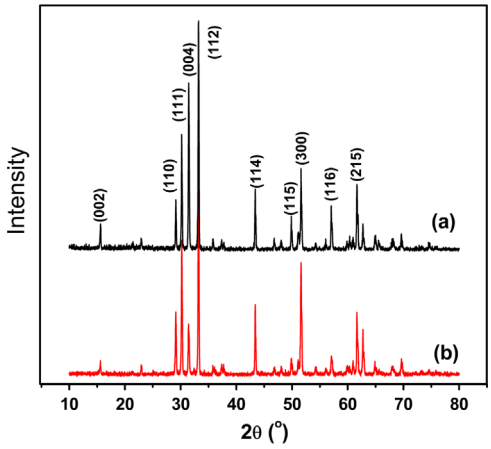

Fig. 7. XRD patterns of YMO obtained by sintering at 1400 °C for 2 h of the powder treated at (**a**) 280 °C for 6 h, and (**b**) 200 °C for 2 h.

secondary phases even when the XRD results show only single-phase pattern.

The thermal evolution of the dc magnetic susceptibility of the single-phase YMO sample is presented in Fig. 9. With decreasing temperature the ZFC and FC magnetic susceptibility curves showed a bifurcation at T_N=43 K below which the ZFC curve showed a maximum. Also, with decreasing temperature the susceptibility increased sharply at about 43 K, indicating a magnetic transition that occurred at this temperature. Temperature of magnetic transition of 43 K is far from typical value of T_N in hexagonal YMO which is about 70 K. Also, the $M(H)$ curve displayed a hysteresis at 5 K confirming the presence of ferro- or ferri-magnetic phase. These phenomena were observed in nanopowders and related to small particle size [8–11] and effect of weak ferromagnetic surface component. In this way the YMO nanoparticles could be treated as core-shell structure, consisting of an antiferromagnetic core and a ferromagnetic shell. According to Zheng and co-authors [11], for nanoparticles with the antiferromagnetic core, the surface spins are expected to dominate magnetic properties. Beside grain size effect, some authors have also connected ferromagnetic properties with non-stoichiometry [15].

According to ICP analysis a pronounced nonstoichiometry was detected in our sample: Mn/Y molar ratio was 1.157

instead of 1. The nonstoichiometry could be treated as the main reason for discrepancy between the theoretical and experimental values measured in our sample. In literature there are examples of Mn self-doping of $YMnO_3$ which gave rise to magnetic hysteresis and drop in Néel temperature with increase in Mn amount [15]. Chen and co-authors obtained the same value of Néel temperature as we did, for the same excess of Mn ions [15].

In order to get better insight in the origin of this magnetic response, the results of the temperature dependence of the reciprocal magnetic susceptibility $\chi^{-1}(T)$ were successfully fitted by a hyperbolic function (Eq. (2)) typical for ferrimagnetic behavior (Fig. 10):

$$\frac{1}{\chi} = \frac{T-\theta_1}{C_{eff}} - \frac{\xi}{T-\theta_2}, \tag{2}$$

where θ_1, C_{eff}, ξ and θ_2 were fitting parameters. Calculated values of the fitting parameters were $\theta_1 = -573$ K, $C_{eff} = 5.13 \cdot 10^{-5}$, $\xi = 1.70 \cdot 10^{8}$, $\theta_2 = 32.8$ K. The negative value of θ_1 confirmed predominant antiferromagnetic interactions. Relative amounts of Mn^{2+} and Mn^{3+} ions can be calculated from fitting parameters using Eq. (3), and taking into account electroneutrality condition:

$$C_{eff} = \frac{N_0 \mu_0 g^2 \mu_B^2}{3k_B} [c_{Mn^{2+}} (S_{Mn^{2+}} (S_{Mn^{2+}} + 1) + c_{Mn^{3+}} (S_{Mn^{3+}} (S_{Mn^{3+}} + 1)] \tag{3}$$

where N_0 denotes the Avogadro constant, μ_o is the permeability of free space, g is the Landé g factor, μ_B is the Bohr magneton, S (Mn^{2+} or Mn^{3+}) is the spin quantum number of Mn^{2+} (Mn^{3+}) ions, c (Mn^{2+} or Mn^{3+}) is the relative concentration of Mn^{2+} (Mn^{3+}) ions and k_B is the Boltzmann constant.

From the calculated relative amounts of Mn^{2+} and Mn^{3+} we can write the formula of our compound as $YMn_{1.152}O_3$, which is in good agreement with the results of the ICP analysis. It should be emphasized that the ferrimagnetic behavior in $YMnO_3$ has been recently, for the first time, reported by Swamy and co-authors [16]. They explained the observed transition from paramagnetic to ferrimagnetic phase of a spin glass type in their samples by spin canting. To the best of our knowledge, that is the only article reporting on the ferrimagnetic properties of undoped $YMnO_3$.

4. Conclusions

Hexagonal single phase $YMnO_3$ nanopowders were successfully synthesized by combination of hydrothermal synthesis and additional thermal treatment. The proposed method is simple and energy efficient. The optimal conditions for

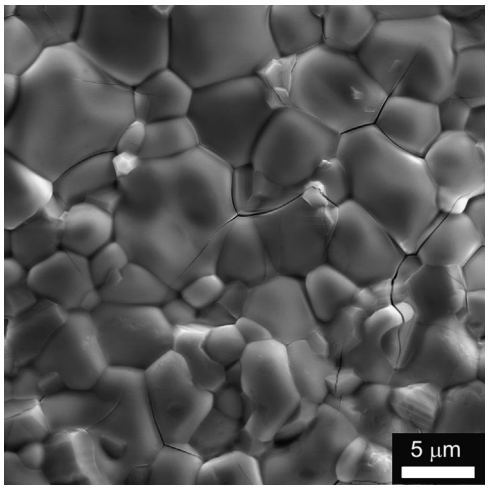

Fig. 8. SEM micrograph of the polished and thermally etched cross-section of the YMO sample sintered at 1400 °C for 2 h.

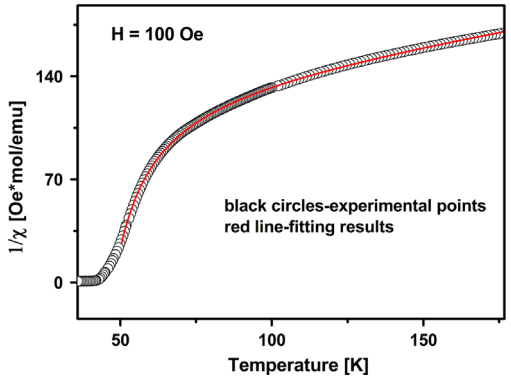

Fig. 10. The temperature dependence of the reciprocal magnetic susceptibility.

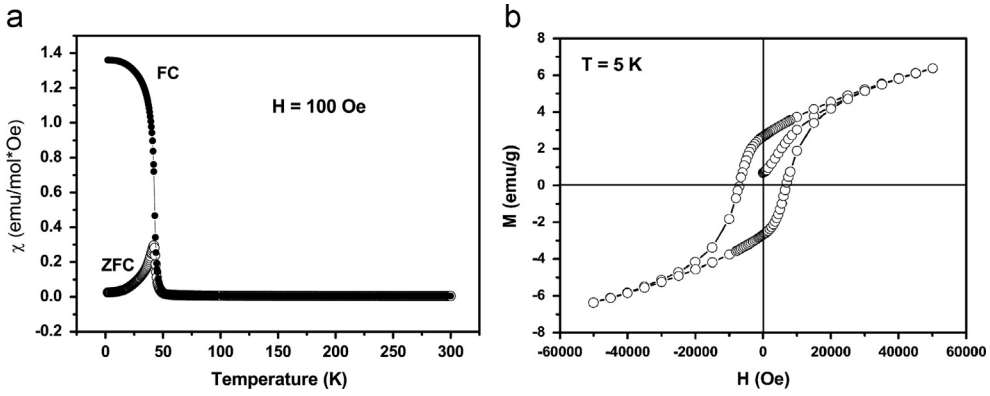

Fig. 9. (**a**) Temperature dependence of the magnetization of $YMnO_3$ ceramics at an applied field of 100 Oe, (**b**) *M–H* hysteresis loop at 5 K.

synthesis of nanopowders were: hydrothermal treatment of solution of starting reagents at 200 °C for 2 h, followed by calcination of the obtained powder at 1200 °C for 2 h. On the other hand, it was shown that calcination step could be skipped in ceramics processing and powders obtained by hydrothermal synthesis were directly pressed and sintered at 1400 °C. The resulting ceramics was single phased, very dense, with homogeneous microstructure, but also nonstoichiometric with excess of Mn of about 15%. Néel temperature of 43 K and magnetic hysteresis confirmed that magnetic properties of the obtained ceramics differed from the expected. Hyperbolic correlation between reciprocal magnetic susceptibility $\chi^{-1}(T)$ and temperature indicated the presence of ferrimagnetic phase, which could be prescribed to the extreme nonstoichiometry.

Acknowledgment

The authors acknowledge that this work was supported by the Ministry of Education, Science and Technological Development of the Republic of Serbia (project number III45007) and Fundação de Amparo à Pesquisa do Estado de Saõ Paulo-FAPESP (project number 2011/00922-0). The authors would like to acknowledge Dr. Biljana Dojčinović – Institute of Chemistry, Technology and Metallurgy, Center of Chemistry, University of Belgrade, Serbia, for providing ICP analysis.

References

[1] D.M. Evans, A. Schilling, A. Kumar, D. Sanchez, N. Ortega, M. Arredondo, R.S. Katiyar, J.M. Gregg, J.F. Scott, Magnetic switching of ferroelectric domains at room temperature in multiferroic PZTFT, Nat. Commun. 4 (2013) 1534, http://dx.doi.org/10.1038/ncomms2548.

[2] W. Eerenstein, N.D. Mathur, J.F. Scott, Multiferroic and magnetoelectric materials, Nature 442 (2006) 759–765.

[3] W. Prellier, M.P. Singh, P. Murugavel, The single-phase multiferroic oxides: from bulk to thin film, J. Phys.: Condens. Matter 17 (2005) R803–R832.

[4] E.S. Stampler, W.C. Sheets, W. Prellier, T.J. Marks, K.R. Poeppelmeier, Hydrothermal synthesis of $LnMnO_3$ (Ln=Ho–Lu and Y): exploiting amphoterism in late rare-earth oxides, J. Mater. Chem. 19 (2009) 4375–4381.

[5] M. Počuča-Nešić, Z. Marinković Stanojević, Z. Branković, P. Cotič, S. Bernik, M. Sousa Góes, B.A. Marinković, J.A. Varela, G. Branković, Mechanochemical synthesis of yttrium manganite, J. Alloy. Compd. 552 (2013) 451–456.

[6] B. Lorenz, Y.Q. Wang, Y.Y. Sun, C.W. Chu, Large magnetodielectric effects in orthorhombic $HoMnO_3$ and $YMnO_3$, Phys. Rev. B. 70 (2004) 212412-1–212412-4, http://dx.doi.org/10.1103/PhysRevB.70.212412.

[7] S.A. Nikolaev, V.G. Mazurenko, A.N. Rudenko, Influence of magnetic order on phonon spectra of multiferroic orthorhombic $YMnO_3$, Solid State Commun. 164 (2013) 16–21.

[8] K. Bergum, H. Okamoto, H. Fjellvåg, T. Grande, M.A. Einarsrud, S. M. Selbach, Synthesis, structure and magnetic properties of nanocrystalline $YMnO_3$, Dalton Trans. 40 (2011) 7583–7589.

[9] M.F. Zhang, J.M. Liu, Z.G. Liu, Microstructural characterization of nanosized $YMnO_3$ powders: the size effect, Appl. Phys. A 79 (2004) 1753–1756.

[10] T.C. Han, W.L. Hsu, W.D. Lee, Grain size-dependent magnetic and electric properties in nanosized $YMnO_3$ multiferroic ceramics, Nanoscale Res. Lett. 6 (2011) 201, http://dx.doi.org/10.1186/1556-276X-6-201.

[11] H.W. Zheng, Y.F. Liu, W.Y. Zhang, S.J. Liu, H.R. Zhang, K.F. Wang, Spin-glassy behavior and exchange bias effect of hexagonal $YMnO_3$ nanoparticles fabricated by hydrothermal process, J. Appl. Phys. 107 (2010) 053901-1–053901-4, http://dx.doi.org/10.1063/1.3296323.

[12] Y. Wang, X. Lu, Y. Chen, F. Chi, S. Feng, X. Liu, Hydrothermal synthesis of two perovskite rare-earth manganites, $HoMnO_3$ and $DyMnO_3$, J. Solid State Chem. 178 (2005) 1317–1320.

[13] C. Moure, J.F. Fernandez, M. Villegas, P. Duran, Non-ohmic behaviour and switching phenomena in $YMnO_3$-based ceramic materials, J. Eur. Ceram. Soc. 19 (1999) 131–137.

[14] M. Tomczyk, A.M. Senos, P.M. Vilarinho, I.M. Reaney, Origin of microcracking in $YMnO_3$ ceramics, Scr. Mater. 66 (2012) 288–291.

[15] W.R. Chen, F.C. Zhang, J. Miao, B. Xu, L.X. Cao, X.G. Qiu, B.R. Zhao, Magnetic properties of the self-doped yttrium manganites $YMn_{1+x}O_3$, J. Phys.: Condens. Matter 17 (2005) 8029–8036.

[16] N.K. Swamy, N.P. Kumar, P.V. Reddy, M. Gupta, S.S. Samatham, D. Venkateshwarulu, V. Ganesan, V. Malik, B.K. Das, Specific heat and magnetocaloric effect studies in multiferroic $YMnO_3$, J. Therm. Anal. Calorim. 119 (2015) 1191–1198, http://dx.doi.org/10.1007/s10973-014-4223-3.